Comparison of Head Injuries as Predicted by Three Different Displacement Velocity Models

Frank B. Tatom and John W. Tatom
Engineering Analysis Inc.
715 Arcadia Circle
Huntsville, AL 35801
(256) 533-9391 Fax (256) 533-9325
fbtatom@mindspring.com jwtatom@mindspring.com

ABSTRACT

Head injuries cause many of the fatalities produced by blast effects. In such injury predictions, the skull is more vulnerable to dynamic pressure than to overpressure. Dynamic pressure, resulting from the blast wave sweeping over the human body, causes the body to be swept along behind the wave at some displacement velocity. Injuries occur when the moving body encounters stationary, solid structures. The displacement velocities for various skull injury levels are known. Solving the motion equation for a body in a transient flow field yields the displacement velocity as a function of peak overpressure and impulse. Baker, et al. and Mercx previously attempted this computation, but in each case significant deficiencies occurred.

In Baker's analysis, both diffraction pressure and drag loading were computed, but the drag on the human body contained no adjustment for the object's motion. Thus, some of Baker's displacement velocities exceeded the particle velocity behind the blast wave, (a physically impossibility), resulting in very inaccurate curves at low peak overpressures (< .4 psi).

In Mercx's analysis diffraction pressure loading was neglected, and in calculating the particle velocity behind the blast wave, Mercx used the ambient air density instead of the density behind the wave. These two deficiencies cause considerable inaccuracy at overpressures above ~10 psi.

In the current Improved Displacement Velocity (IDV) analysis, the effects of both diffraction pressure-loading and drag-loading were considered, with allowance for the body's displacement velocity, and with the correct air density used in the particle velocity equation.

Pressure-impulse diagrams were calculated based on all three methods for four displacement velocities (corresponding to four fracture probabilities). At low pressures the IDV curves closely match Mercx's while lying well above Baker's. Between 3 and 10 psi the IDV curves generally agree with Baker's, as Mercx's drift to the right. The IDV curves extend to pressures as high at 1000 psi, while Baker's curves end at ~10 psi, and Mercx's at ~100 psi. A comparison of results has revealed that the IDV model represents a bridge between the two earlier models, eliminating the major deficiencies associated with each.

Report Documentation Page

Form Approved
OMB No. 0704-0188

1. REPORT DATE	2. REPORT TYPE	3. DATES COVERED
AUG 1998		**00-00-1998 to 00-00-1998**

4. TITLE AND SUBTITLE	5a. CONTRACT NUMBER
Comparison of Head Injuries as Predicted by Three Different Displacement Velocity Models	5b. GRANT NUMBER
	5c. PROGRAM ELEMENT NUMBER
6. AUTHOR(S)	5d. PROJECT NUMBER
	5e. TASK NUMBER
	5f. WORK UNIT NUMBER
7. PERFORMING ORGANIZATION NAME(S) AND ADDRESS(ES) **Engineering Analysis Inc,715 Arcadia Circle,Huntsville,AL,35801**	8. PERFORMING ORGANIZATION REPORT NUMBER
9. SPONSORING/MONITORING AGENCY NAME(S) AND ADDRESS(ES)	10. SPONSOR/MONITOR'S ACRONYM(S)
	11. SPONSOR/MONITOR'S REPORT NUMBER(S)

12. DISTRIBUTION/AVAILABILITY STATEMENT
Approved for public release; distribution unlimited

13. SUPPLEMENTARY NOTES
See also ADM001002. Proceedings of the Twenty-Eighth DoD Explosives Safety Seminar Held in Orlando, FL on 18-20 August 1998.

14. ABSTRACT
see report

15. SUBJECT TERMS

16. SECURITY CLASSIFICATION OF:			17. LIMITATION OF ABSTRACT	18. NUMBER OF PAGES	19a. NAME OF RESPONSIBLE PERSON
a. REPORT **unclassified**	b. ABSTRACT **unclassified**	c. THIS PAGE **unclassified**	**Same as Report (SAR)**	**6**	

1.0 INTRODUCTION

Most analyses dealing with the blast effects produced by explosions are primarily concerned with the prediction of damage to inanimate structures. In many cases, however, the ultimate purpose of such analyses has been the prevention of injury to personnel. For this reason, as part of a company-funded research program, a literature survey was conducted, dealing with the vulnerability of the human body to blast [1-12]. As part of this research special attention was given to the human skull. Two models for predicting blast injuries to the skull were identified [7, 10]. Comparison of the predicted injury levels produced by the two models revealed significant differences. A careful review of the two analytical approaches, including contact with the authors, or co-authors, confirmed certain deficiencies in each technique. To resolve the differences in the two previous models, the Improved Displacement Velocity (IDV) model was developed by EAI.

2.0 DEVELOPMENT OF IMPROVED DISPLACEMENT VELOCITY MODEL

In calculating personnel injury due to blast, the vulnerability of the skull is of special importance. As the blast wave envelopes the human body, the body begins to be swept along at some displacement velocity. Under such conditions injury to the skull, like injury to other bones, is considered to result primarily from the impact with a solid, stationary object. For this reason, skull vulnerability is generally expressed as a function of displacement velocity, as shown in Table 1.

Table 1. Skull Vulnerability [3, 4, 6]

Displacement Velocity (ft/sec)	Fracture Probability (%)
10	0
13	1
18	50
23	99

Calculation of the maximum displacement velocity is thus the fundamental step in establishing skull vulnerability. The basic problem can be described as the calculation of the motion of an immersed object in a transient, compressible, one-dimensional flow field. The basic governing equation can be written as

$$m\, dV/dt = F_{drag} + F_{diff} \tag{1}$$

where

m = mass of human body

V = displacement velocity of human body

t = time

F_{drag} = drag load

F_{diff} = diffraction load

Now,

$$F_{drag} + F_{diff} = P_r A \qquad (t \le t_s) \tag{2}$$

$$F_{drag} = C_D \rho_s (U_s - V) \mid U_s - V \mid A / 2 \qquad (t \ge t_s) \tag{3}$$

$$F_{diff} = \begin{cases} K_s A & (t_s \le t \le t_d) \\ 0 & (t > t_d) \end{cases} \tag{4}$$

where

P_r = reflected overpressure

C_D = drag coefficient (1.3) [13]

ρ_s = gas density behind shock

U_S = gas velocity behind shock

P_S = gas overpressure behind shock

A = projected area of human body

t_S = rise time to reach stagnation pressure

t_d = rise time to reach peak overpressure

According to compressible fluid flow fundamentals [14],

$$P_r = 2 P_S (7 P_\infty + 4 P_S) / (7 P_\infty + P_S) \quad (5)$$

$$\rho_S = \rho_\infty (7 P_\infty + 6 P_S) / (7 P_\infty + P_S) \quad (6)$$

$$U_S = 5 C_\infty P_S / \sqrt{7 P_\infty (7 P_\infty + 6 P_S)} \quad (7)$$

$$C_\infty = \sqrt{\gamma R T_\infty} \quad (8)$$

where

P_∞ = ambient pressure

C_∞ = ambient speed of sound

γ = specific heat ratio for air (1.4)

R = specific gas constant for air

T_∞ = ambient air temperature

According to Glasstone [15],

$$P_S = P_o (1 - t / t_p) \quad (9)$$

$$t_s = 3\ w / 2 / U_s \quad (10)$$

$$t_d = (b + 4w / 2) / U_s \quad (11)$$

where

P_o = peak overpressure

t_p = positive phase duration

w = width of human body

b = thickness of human body

Now, if P_s varies linearly with time, the duration of the positive phase can be expressed as

$$t_p \cong 2\ I_{pp} / P_o \quad (12)$$

where

I_{pp} = impulse for positive phase

Inspection of the preceding equations reveals that for constant values of m (mass), A (projected area), w (width), and b (thickness) of the human body the displacement velocity, V, can be expressed as a function of the two variables, P_o and I_{pp}. Thus, the displacement velocity can be expressed in the form of a pressure-impulse (P-I) diagram.

As part of two earlier studies [7, 10], attempts were made to solve the problem of calculating the displacement velocity of the human body. Because of significant discrepancies in each attempt, however, the results are not in agreement. In the first attempt, Baker et al [7], in calculating drag, did not take into account the changing displacement velocity as a function of time. Baker's model is especially important because it has been accepted by the Department of Energy [12] and is commonly used by the Department of Defense [16].

Mercx [10] used an unrealistically low drag coefficient, neglected diffraction loading altogether, and also used the ambient air density instead of shock gas density in

calculating gas velocity behind the shock. Mercx's model is noteworthy because it is commonly used by the oil and gas industry, especially in Europe.

The effects of the deficiencies in the two models are noted in subsequent discussion. Eqs. (1) through (12), as formulated, resolve such deficiencies and constitute the Improved Displacement Velocity (IDV) model. Numerical solution of the IDV model equations was accomplished by means of the EAI SWEEP software for pressures ranging from .01 to 1000 psi and impulses ranging from 1 to 10^7 psi ms. The results were then plotted in the form of a P-I diagram for purposes of comparison with the results produced by Baker's and Mercx's models, as described in Section 3.0

3.0 COMPARISON OF RESULTS

In order to compare the results produced by the three models a series of calculations were carried out for the case of 6-foot tall, 180-pound man. The resulting pressure-impulse diagrams based on Baker's model, Mercx's model, and the IDV model are presented in subsections 3.1, 3.2, and 3.3 respectively. The differences in the predicted vulnerabilities are discussed in subsection 3.4.

3.1 BAKER'S MODEL RESULTS

Based on Baker's model, the four displacement velocities given in Table 1 can be represented by a family of four curves on a pressure impulse diagram, as shown in Figure 1. In this diagram the abscissa is peak overpressure, P_o, and the ordinate is positive phase impulse, I_{pp}. Examination of Figure 1 reveals the effect of neglecting the changing displacement velocity as a function of time in calculating drag. From the basic principle of compressible fluid flow the gas velocity can be expressed as a function of overpressure as given by Eq. (7). For typical atmospheric conditions [17].

$P_\infty = 14.6941$ psia

$T_\infty = 531.69\ ^\circ R$

$R_\infty = 53.36$ ft-lbf/(ft-lbm$^\circ$ R)

With these values introduced into Eq. (7), the maximum gas velocity behind the shock

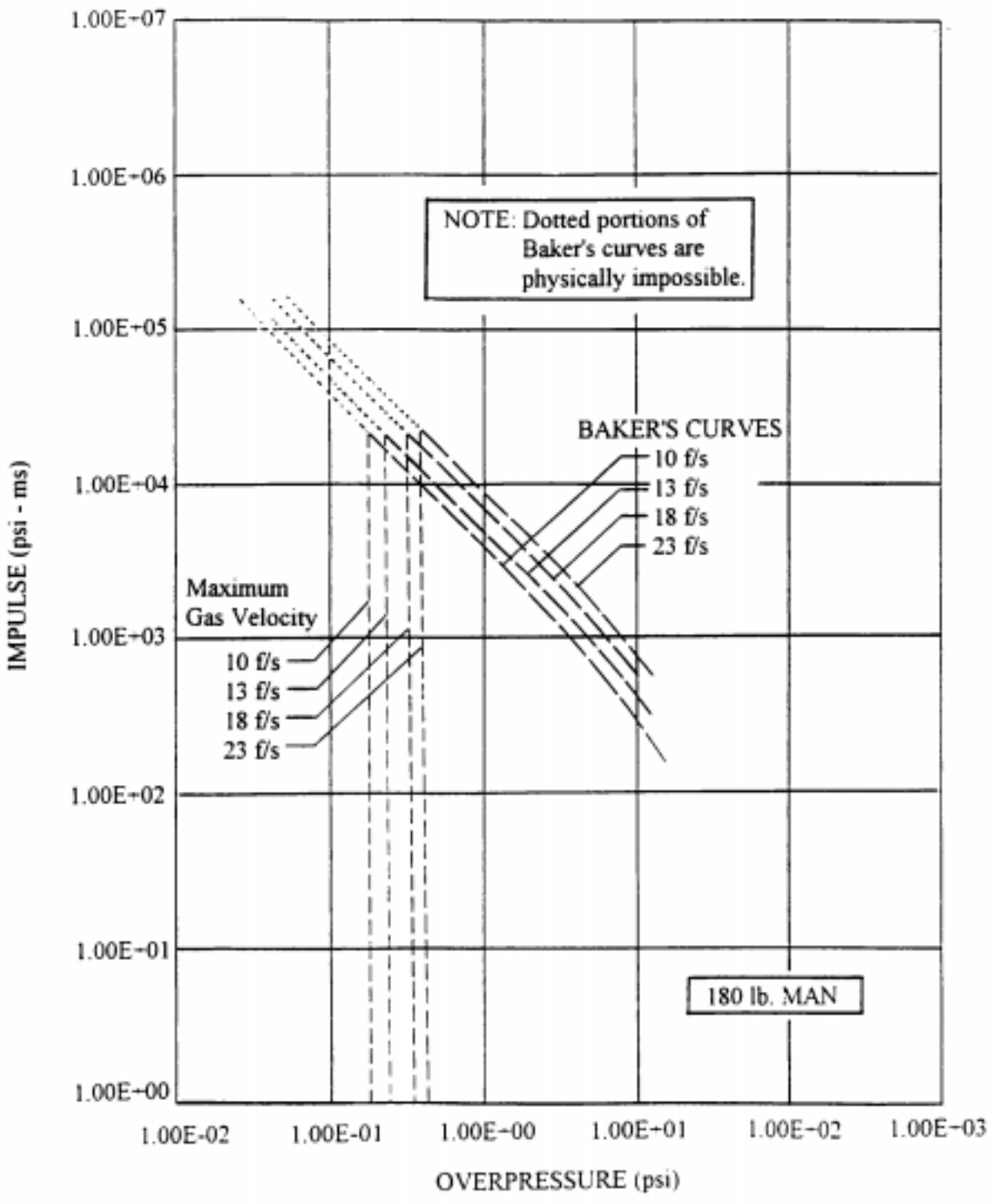

Figure 1. Pressure-Impulse Diagram for Human Skull According to Baker's Model [7]

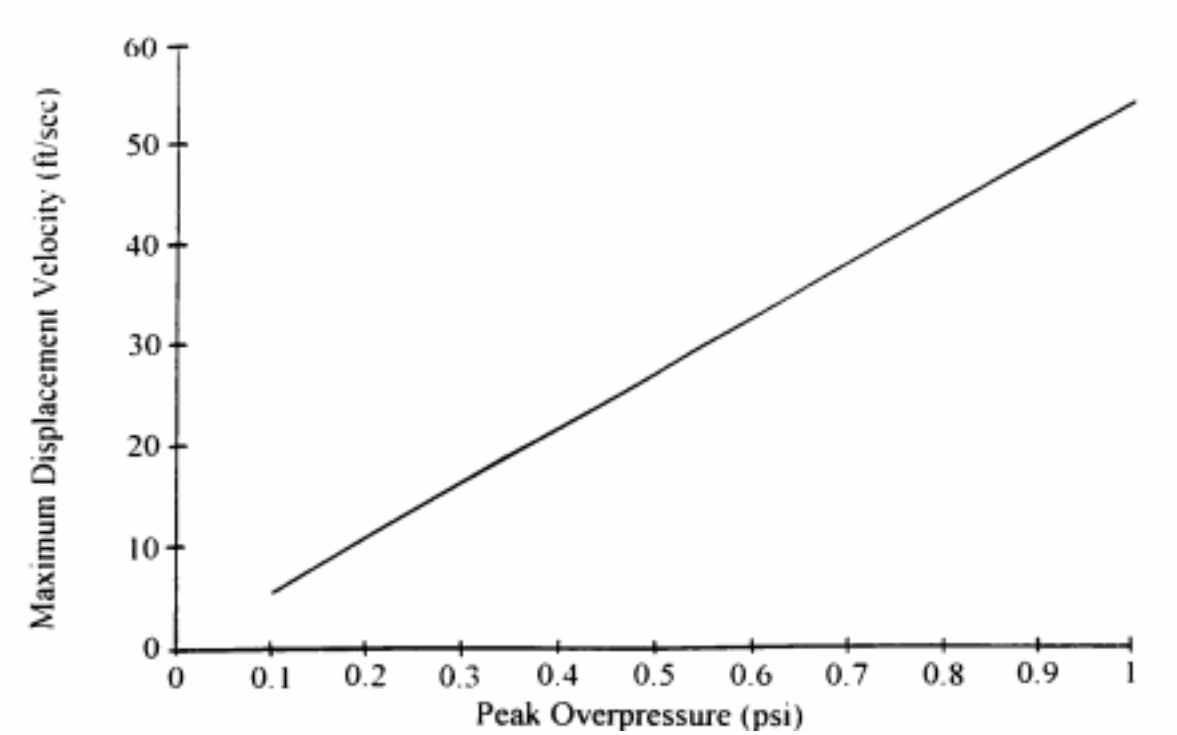

Figure2. Maximum Diplacement Velocity as a Function of Peak Overpressure (0.1-1.0 psi)

can be represented as function of the peak overpressure, P_o, as shown in Figure 2. Now the maximum displacement velocity cannot exceed the maximum gas velocity behind shock, especially for low pressures and large impulses. Thus, based on Figure 2, for each of the four displacement velocities there is a minimum overpressure below which the dis-placement velocity cannot occur. These minimum overpressures are tabulated in Table 2.

As indicated in Figure 1, when these minimum overpressures are taken into account, the upper one-third of Baker's curves are physically impossible. **Thus, Baker's curves greatly over-estimate the injury to the skull for low pressures (< .5 psi) and large impulses (> 20,000 psi-ms).**

Table 2. Minimum Peak Overpressures

Displacement Velocity (ft/sec)	Minimum Peak Overpressure (psi)
10	.1829
13	.2382
18	.3307
23	.4237

3.2 MERCX'S MODEL RESULTS

In the case of Mercx, the four displacement velocities can also be represented as a family of four curves on a pressure-impulse diagram, as shown in Figure 3. Comparison of these curves with Baker's curves reveals a general difference in shape. For equal displacement velocities close inspection reveals that the curves do not intersect, with Mercx's curves always lying above and to the right of Baker's. No physically obvious discrepancy can be detected by simple inspection, but the fact that Mercx's curves share no common points with Baker's is interesting. For low pressures the difference in the curves results from the deficiency in Baker's drag calculations. At higher pressures the difference is caused primarily by Mercx's use of an unrealistically low drag coefficient (~.75) and his neglect of diffraction loading on the body. **For these higher pressures Mercx's curves tend to underestimate the vulnerability of the skull.**

3.3 IDV MODEL RESULTS

By means of the IDV model, the four displacement velocities produce four curves in the P-I diagram shown in Figure 4. Close inspection reveals that a low pressure and larger impulse the IDV curves closely match Mercx's while at higher pressure sand low impulse the IDV curves agree fairly well with Baker's. This pattern is clearly shown in Figure 5 for the 18 ft/sec displacement velocity curve. **Thus, the IDV curves at low pressures generally result in lower vulnerability, when compared with Baker's, and at high pressures result in greater vulnerability, when compared with Mercx's.** These results are completely consistent with the more rigorous formulation of the problem associated with the IDV model.

In order to increase their utility the IDV curves for the skull have been incorporated into the Vulnerability Assessment of Structurally Damaging Impulses and Pressures, (VASDIP) 3.0 software [18]. Similar curves for eighteen other components of the human body are also included in the software.

3.4 DIFFERENCES IN VULNERABILITY PREDICTIONS

To demonstrate the vulnerability differences produced by the three models, a series of calculations were carried out along the IDV 18 ft/sec curve, corresponding to 50% injury.

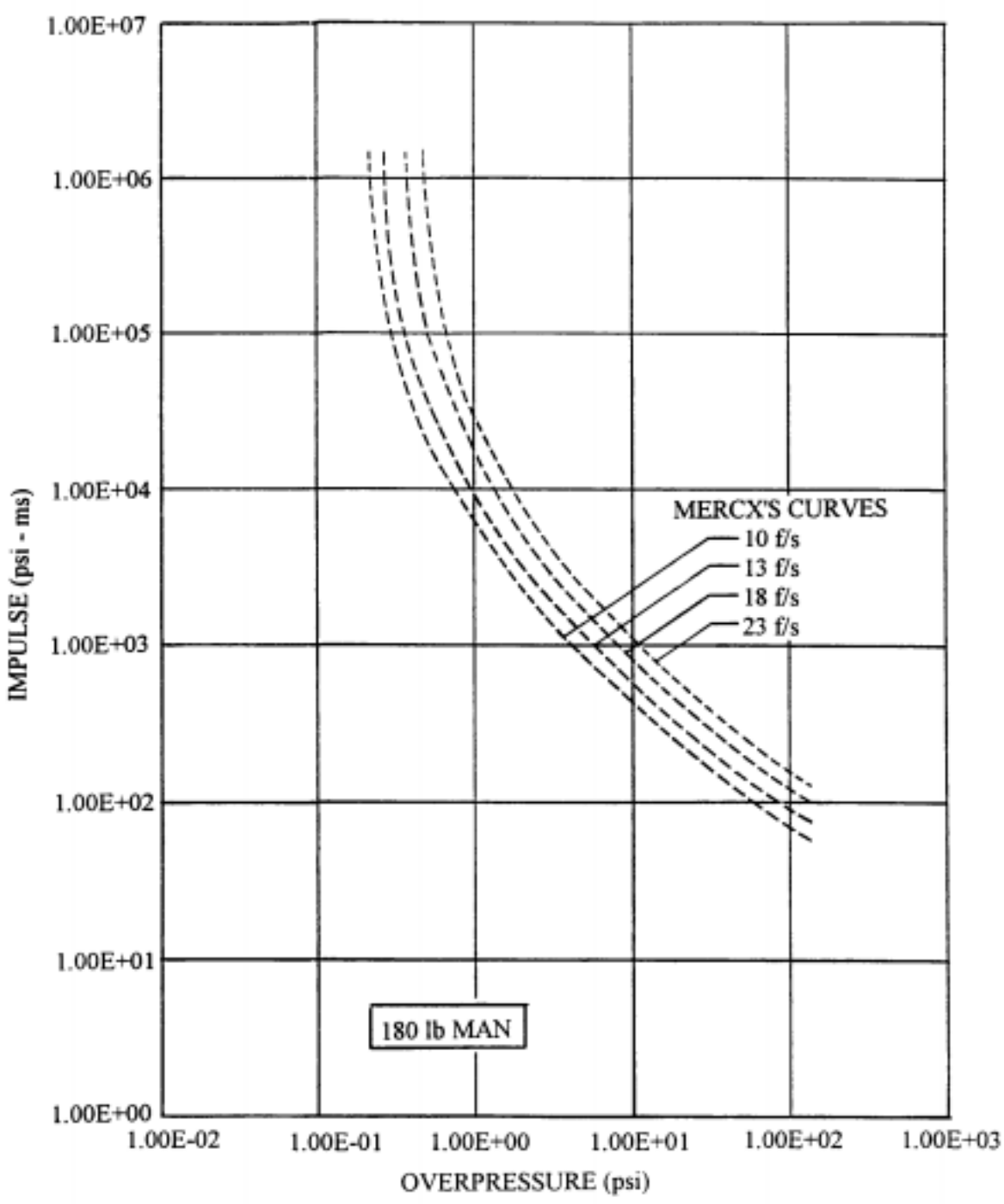

Figure 3. Pressure-Impulse Diagram for Human Skull According to Mercx's Model

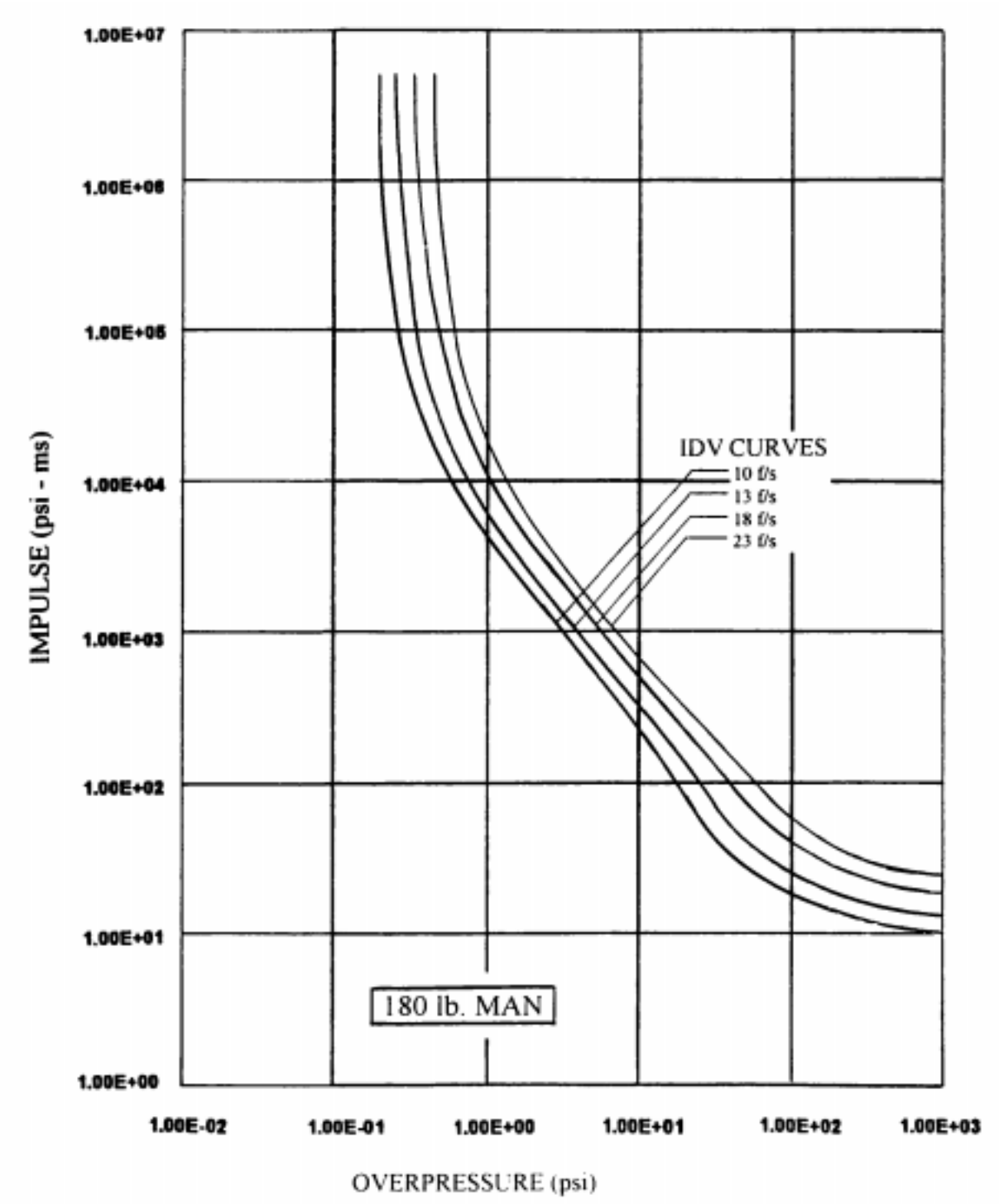

Figure 4. Pressure-Impulse Diagram for Human Skull According to IDV Model

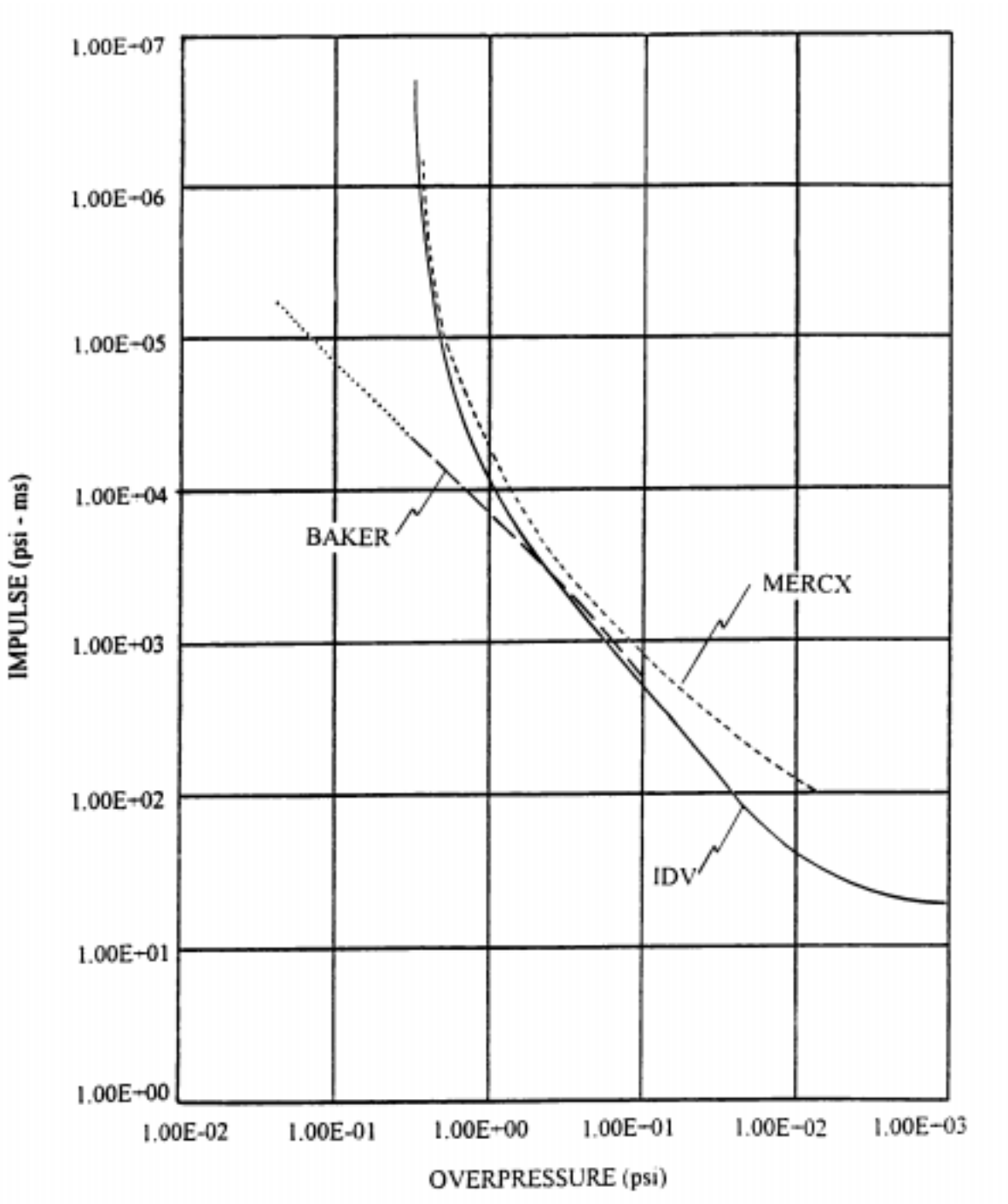

Figure 5. Comparison of Pressure-Impulse Diagram for 18 ft/sec Displacement Velocity

The results are shown in Table 3 and Figure 6. Again these results reinforce the statements already made concerning the inaccuracies associated with both Baker's and Mercx's models. Agreement between all three curves is not achieved at any point along the plot. While these differences do not appear to be that great when comparing the families of curves on P-I diagrams, **the differences in vulnerability as given in Table 3 and Figure 6 differ by as much as 80%**.

Table 3. Comparison of Predicted Vulnerability Along IDV 18 ft/sec Curve

Overpressure (psi)	Impulse (psi ms)	Vulnerability (%)		
		Baker	Mercx	IDV
0.5	83,619	100	50	50
1	11,445	100	19	50
2	3,758	66	18	50
5	1,162	31	7	50
10	511.2	36	0.7	50
20	222.1	---	0	50
50	72.53	---	0	50
100	39.59	---	0	50
200	26.48	---	---	50
500	20.07	---	---	50
1000	17.37	---	---	50

4.0 CONCLUSIONS

The two most commonly used models for skull vulnerability [7, 10] each suffer from significant deficiencies which result in vulnerability values which consistently differ from one another from 25 to 80%. The more recent IDV model was designed to overcome the deficiencies associated with the two earlier models, and the results demonstrate that the IDV model serves as a bridge between the earlier two. **Because of the importance of skull injuries in predicting blast effects on the human body, the use of the IDV model, as incorporated into the VASDIP 3.0 software [18], should significantly improve the accuracy of such injury predictions.**

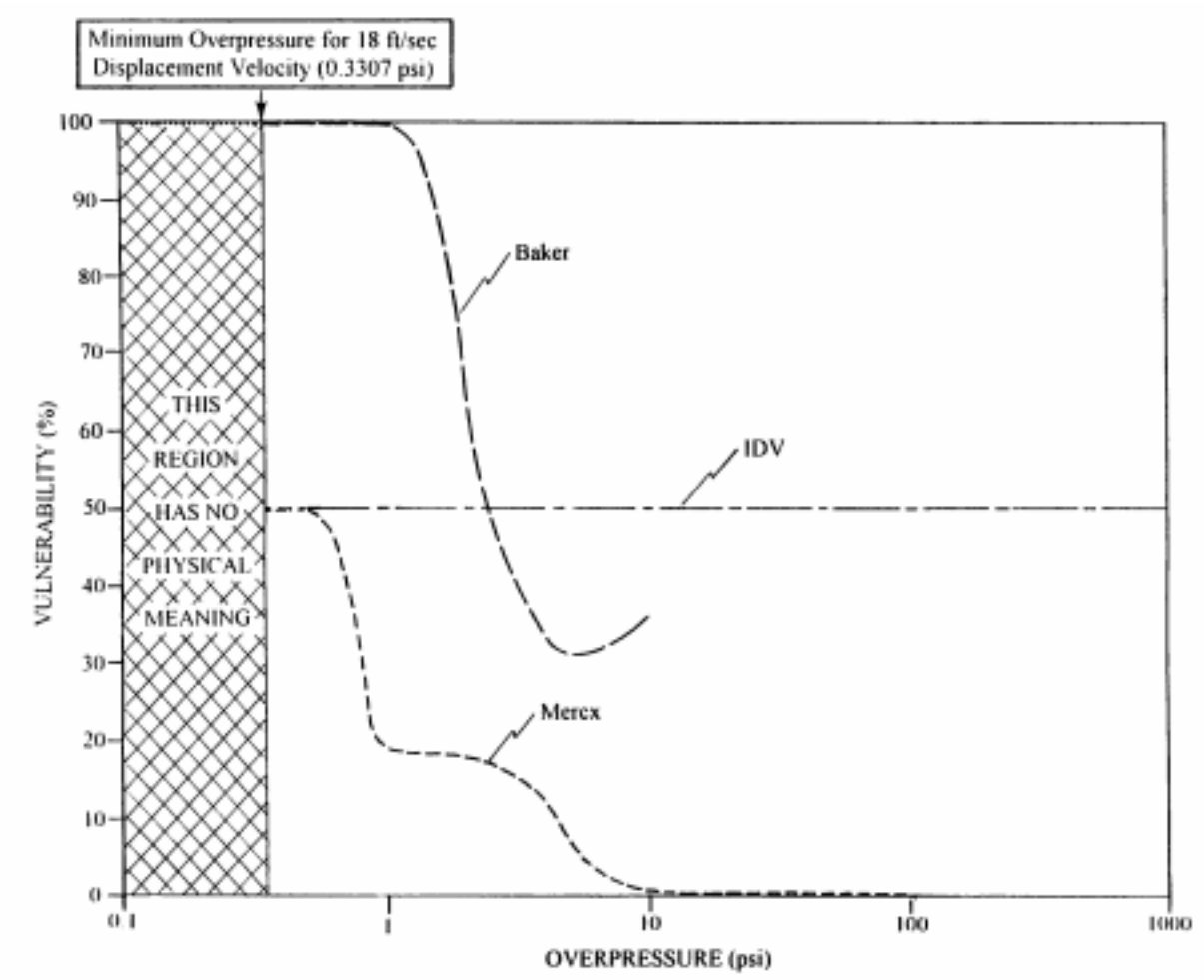

Figure 6. Predicted Vulnerability Along IDV 18 ft/sec Curve

5.0 REFERENCES

1. Richmond, D. R., Damon E.G., Fletcher, E. R., Bowen, I.G., and White C.S., "The Relationship Between Selected Blast-Wave Parameters and the Response of Mammals Exposed to Air Blast", Annals of the New York Academy of Sciences, Vol. 152, Art. 1, pp. 1034, October 1968.

2. Bowen, I.G., Fletcher, E.R., and Richmond, D.R., "Estimate of Man's Tolerance to the Direct Effects of Air Blast", AD 693105, Technical Report to Defense Atomic Support Agency, DASA 2113, Lovelace Foundation for Medical Education and Research, October 1968.

3. White, C.S., "The Scope of Blast and Shock Biology and Problem Areas in Relating Physical and Biological Parameters", Annals of the New York Academy of Sciences, Vol. 152, Art. 1, pp. 89-102, October 1968.

4. Clemedson, C.J., Hellstrom, G., and Lingren, S., "The Relative Tolerance of the Head, Thorax, and Abdomen to Blunt Trauma", Annals of the New York Academy of Sciences, Vol. 152, Art. 1, pp. 187+, October 1968.

5. Damon, E.G., Yelverton, J.T., Luft U.C., Mitchell K., and Jones, R.K., "The Acute Effects of Air Blast on Pulmonary Function in Dogs and Sheep", AD 709972, Technical Progress Report to Defense Atomic Support Agency, DASA 2461, Lovelace Foundation for Medical Education and Research, March 1970.

6. White, C.W., Jones, R.K., Damon, E.G., Fletcher, E.R., and Richmond, D.R., "The Biodynamics of Air Blast", Technical Report to Defense Nuclear Agency, DNA 2738T, Lovelace Foundation for Medical Education and Research, AD 734 208, July 1971.

7. Baker, W.E., Kulesz, J.J., Ricker, R.E., Bessey, R.L., Westine, P.S., Parr, V.B., and Oldham, G.A., "Workbook for Predicting Pressure Wave and Fragment Effects of Exploding Propellant Tanks and Gas Storage Vessels", NASA CR-134906, November 1975.

8. Stull, Daniel R., Fundamentals of Fire and Explosion, American Institute of Chemical Engineers Monograph Series, No. 10, Volume 73, 1977.

9. "Hazards of Chemical Rockets and Propellants", CPIA Publication 394, Vol. 1, Chemical Propulsion Information Agency, The Johns Hopkins University, Applied Physics Laboratory, Laurel, Maryland, September 1984.

5.0 REFERENCES (cont.)

10. Mercx, W. Paul, "Chapter 3. The Consequences of Explosion Effects on Humans", contained in Methods for the Determination of Possible Damage to People and Objects Resulting From Releases of Hazardous Materials, CPR 16E, The Director-General of Labour, Voorburg, The Netherlands, December 1989.

11. Structures to Resist the Effects of Accidental Explosions, Department of the Army Technical Manual TM 5-1300, Department of the Navy Publication NAVFAC P-397, Department of the Air Force Manual AFM 88-22, Department of the Army, The Navy, and the Air Force, Revision 1, November 1990.

12. "A Manual for the Prediction of Blast and Fragment Loadings on Structures", DOE/TIC-11268, Department of Energy, Albuquerque Operations Office, February 1992.

13. Hoerner, Sighard F., Fluid-Dynamic Drag, Published by the Author, Midland Park, New Jersey, 1958.

14. Shapiro, Ascher H., The Dynamics and Thermodynamics of Compressible Fluid Flow, Vol.1, The Ronald Press Company, New York, 1953.

15. Glasstone, S., and Dolan, P. J., The Effects of Nuclear Weapons, United States Department of Defense and the Energy Research and Development Administration, U.S. Government Printing Office, Washington, D.C., 1977.

16. Lahoud, Paul, personal communication, U.S. Army Corps of Engineers, June 8, 1998.

17. U.S. Standard Atmosphere, 1962, U.S. Government Printing Office, Washington, D.C., December 1962.

18. Tatom, F.B., and Tatom, J.W., "Vulnerability Assessment of Structurally Damaging Impulses and Pressures, Third Version (VASDIP 3.0) Users Manual", EAI-TR-97-007, Engineering Analysis Inc., Huntsville, AL, March 1997.